

Motility-Induced Pinning in Flocking System with Discrete Symmetry

Chul-Ung Woo and Jae Dong Noh

Department of Physics, University of Seoul, Seoul 02504, Korea

(Dated: March 18, 2024)

We report a motility-induced pinning transition in the active Ising model for an active self-propelled particle system with discrete symmetry. This model was known to exhibit a liquid-gas type flocking phase transition, but a recent study reveals that the polar order is metastable due to droplet excitation. Using extensive Monte Carlo simulations, we demonstrate that, for an intermediate alignment interaction strength, the steady state is characterized by traveling local domains, which renders the polar order short-ranged in both space and time. We further demonstrate that interfaces between colliding domains become pinned as the alignment interaction strength increases. A resonating back-and-forth motion of individual self-propelled particles across interfaces is identified as a mechanism for the pinning. We present an analytic argument for the motility-induced pinning transition by incorporating the resonance mechanism into the hydrodynamic theory. The resulting steady state consists of a network of pinned interfaces interconnected by particle currents. While the polar order is still short-ranged in space, the particle currents mediated by the pinned interfaces can exhibit long-range temporal correlations.

Introduction – Active matter, consisting of self-propelled particles (SPPs), displays intriguing collective phenomena [1, 2]. SPPs, such as migrating cellular organisms [3–5], swarming animals [6–11], synthetic materials [12–15], and so on, convert internal or external energy into kinetic motion. The self-propulsion distinguishes active matter from thermal equilibrium systems. When SPPs interact through local velocity alignment, they can exhibit long-range polar order with broken continuous symmetry, even in two dimensions [16, 17]. This is in contrast to thermal equilibrium systems, where the Mermin-Wagner theorem prohibits such ordering [18]. Repulsive interactions among SPPs can lead to a phase separation, whereas attractive interactions would be necessary in thermal equilibrium systems [19–22]. Active matter systems incorporating other elements, such as discrete symmetry [23–29], multiple species [30–32], and quenched disorder [33–36], have been attracting growing interest.

The Vicsek model is a well-established model for the flocking transition [16]. It comprises SPPs whose self-propulsion direction is represented by a continuous XY spin variable. Both a field-theoretic renormalization group study [17, 37] and extensive numerical simulations confirm that the model indeed exhibits the long-range polar order [38–44]. However, controversy existed regarding the nature of the phase transition, whether it is continuous or discontinuous. This issue was resolved using the framework of the active Ising model (AIM) with discrete symmetry [24, 45, 46]. As a discrete model, it enables large scale numerical simulations and facilitates an analytically tractable hydrodynamic theory. The system has been known to exhibit a liquid-gas type phase transition between a disordered (gas) phase and a polar ordered (liquid) phase. These phases are separated by a coexistence phase where particles are phase separated into gas and liquid regions. The liquid region forms a macroscopic band traveling over the gaseous background. The

liquid-gas transition picture has also been confirmed in the Vicsek model with a modification that macrophase separation is replaced with microphase separation in the coexistence phase [46].

Recent studies have revealed the fragility of the long-range polar order in active matter systems. In the Vicsek model, a single point-like obstacle or a finite counter-propagating blob can disrupt the global polar order [47]. The AIM exhibits even greater fragility [48]. When the system is prepared in an ordered state, droplet excitations spontaneously nucleate and counter-propagate at a constant speed, ultimately destroying the initial polar order. These findings raise an interesting question: does the long-range polar order truly exist in the active matter systems with discrete symmetry? If not, what would be the asymptotic phase?

This Letter addresses those questions specifically in the context of the AIM. We demonstrate numerically that both the ordered and the coexisting states in the liquid-gas transition scenario ultimately evolve to a state consisting of randomly oriented finite-size traveling droplets, rendering the polar order short-ranged in both space and time. Interestingly, we discover as the alignment interaction strength increases further, the system undergoes a *motility-induced pinning* (MIP) transition instead of the expected liquid-gas transition. In the pinned phase, interfaces between domains oriented in opposite directions become immobile. Individual particles accumulate near these interfaces and exhibit a back and forth resonating motion. We will provide a numerical evidence for the MIP and its analytic justification based on the hydrodynamic theory, and discuss the implication on the polar order.

Active Ising model – The AIM [24] comprises N SPPs on a two-dimensional (2D) lattice of $L_x \times L_y$ sites with periodic boundary conditions. The overall density is denoted as $\rho_0 = N/(L_x L_y)$. Each particle is associated with an Ising spin variable, $s = \pm 1$, indicating its self-propulsion

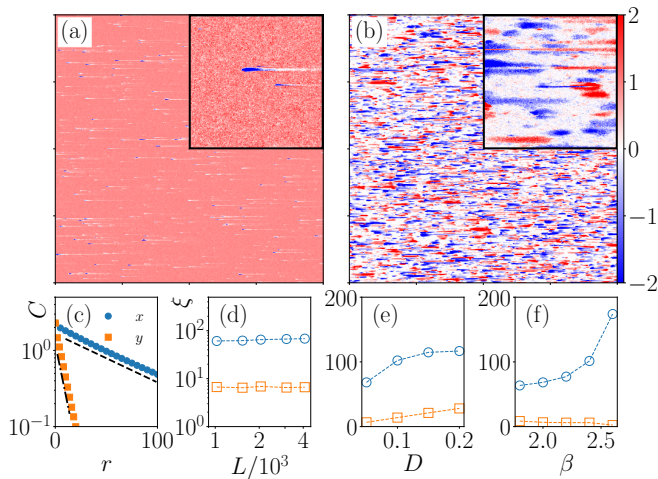


FIG. 1. Snapshots taken at 4×10^3 MCSs in (a) and at 5×10^4 MCSs in (b) after starting from an ordered initial configuration. The insets present an enlarged view of a subsystem of size 256×256 . The normalized magnetization m/ρ_0 is color-coded according to the color bar. (c) Magnetization correlation functions in the steady state along the x and y directions (symbols). They follow an exponential decay (dashed lines) with characteristic sizes $\xi_x > \xi_y$. Parameters values are $L_x = L_y = 4096$, $\rho_0 = 8$, $D = 0.05$, $v = 1$, and $\beta = 2$. Also shown are dependence of ξ_x (circles) and ξ_y (squares) on the system size in (d), the diffusion rate in (e), and the inverse temperature (f).

direction (right or left). Particles hop to one of their four neighbors at diffusion rate $4D$, self-propel to a neighboring site on the right ($s = +1$) or left ($s = -1$) at rate v , and can flip their spin state ($s \rightarrow -s$) at rate $w e^{-\beta s m_{\mathbf{r}}/\rho_{\mathbf{r}}}$, where $\rho_{\mathbf{r}}$ and $m_{\mathbf{r}}$ denote the number of particles and the magnetization at the residing site $\mathbf{r} = (x, y)$, respectively. The ratio $p_{\mathbf{r}} = m_{\mathbf{r}}/\rho_{\mathbf{r}}$ is called the polarization at site \mathbf{r} . We will set $w = 1$. The parameter β , called the inverse temperature, represents a strength of an alignment interaction of self-propulsion directions. The polar order manifests itself as a ferromagnetic order of the Ising spin variables.

The AIM can be described by the continuum hydrodynamic equation, based on a local mean-field approximation, for the density field $\rho = \rho(\mathbf{r}, t)$ and the magnetization field $m = m(\mathbf{r}, t)$ [45, 48]:

$$\begin{aligned} \partial_t \rho &= \nabla \cdot D \nabla \rho - v \partial_x m \\ \partial_t m &= \nabla \cdot D \nabla m - v \partial_x \rho + F(\rho, m) \end{aligned} \quad (1)$$

Here, $F(\rho, m) = 2\rho \sinh(\beta m/\rho) - 2m \cosh(\beta m/\rho)$, and the diffusion matrix D is diagonal with elements $D_x = D + v/2$ and $D_y = D$.

We have simulated the AIM dynamics using a parallel update Monte Carlo method. During one Monte Carlo sweep (MCS), corresponding to a time interval $\Delta t = 1/(4D + v + e^\beta)$, all particles attempt hopping, self-propulsion, or spin flip in parallel [49].

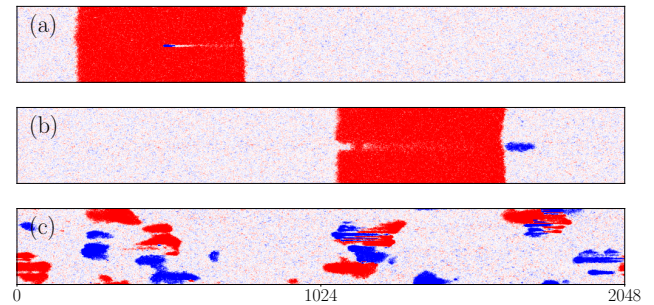


FIG. 2. Time evolution from a phase-separated initial configuration [50]. (a) A droplet nucleates and propagates within the ferromagnetic band. (b) The droplet is about to collide with the band again in 7×10^3 MCS since the snapshot (a) was taken. (c) A steady state configuration in 6×10^4 MCSs since (b). The magnetization is color-coded as in Fig. 1. Parameters: $L_x = 2048$, $L_y = 256$, $\rho_0 = 3$, $D = 0.1$, $v = 1$, and $\beta = 2$.

Metastability of ordered and coexistence phases – We confirm the metastability of the ordered state (see Fig. 1), which was first reported in Ref. [48]. The system, starting from an ordered initial state, evolves into a state with multiple traveling droplets, nucleated spontaneously. These droplets grow and merge into larger ones. At the same time, they also suffer from spontaneous nucleation of droplets of opposition polarization, and break up into smaller pieces. This competition between growth and break-up drives the system to a steady state with randomly distributed local domains [50].

The characteristic size of droplets is estimated using the correlation function $C(\mathbf{r}) := \sum_{\mathbf{r}_0} \langle m_{\mathbf{r}+\mathbf{r}_0} m_{\mathbf{r}_0} \rangle_{ss} / (\rho_0^2 L_x L_y)$, where $\langle \rangle_{ss}$ denotes a steady state time average. As shown in Fig. 1(c), it decays exponentially with distance in both x and y directions. Importantly, the characteristic sizes ξ_x and ξ_y converge to finite values as the system size increases (Fig. 1(d)). Additionally, the characteristic sizes vary smoothly with other parameters like D and β (Fig. 1(e, f)). These observations collectively indicate that the polar order in the steady state is short-ranged in both space and time.

The coexistence phase is also found to be metastable, as illustrated in Fig. 2. When one starts with a configuration with macrophase separation, a droplet nucleates spontaneously inside a band. It grows to a size of $\xi = O(L_x)$ before escaping the band. Continuing its ballistic movement, it evaporates as constituent particles diffuse out into the disordered background. Notably, this diffusive evaporation process would take a time $\tau_{\text{evap}} \sim \xi^2 = O(L_x^2)$, while collision with the band takes $\tau_{\text{col}} = O(L_x)$. Therefore, in sufficiently large systems where $\tau_{\text{evap}} \gg \tau_{\text{col}}$, the droplet repeatedly invades the band (Fig. 2(b)), ultimately destroying it. Figure 2(c) shows the resulting steady-state configuration, where fi-

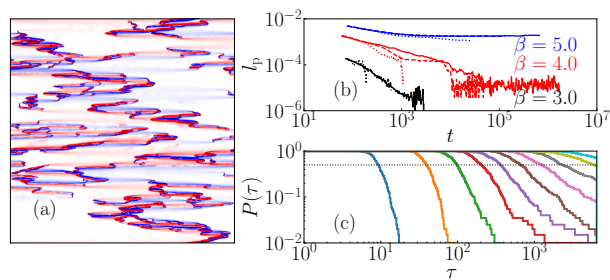


FIG. 3. (a) Snapshot taken at 10^7 MCS starting from a random initial configuration at $\beta = 5$ ($L = L_x = L_y = 4096$) [50]. The normalized magnetization is color-coded as in Fig. 1. (b) Total length of pinned interface segments along the y axis, normalized by the system size L^2 , for different values of β and $L = 256$ (dotted), 512 (dashed), 1024 (solid). (c) Survival probability of an isolated droplet of radius $r_0 = 2, 4, \dots, 20$ (from left to right) on a rectangular lattice of size 2048×256 at $\beta = 5.0$. The characteristic life time $\tau(r_0)$, at which the survival probability reaches $1/2$ (dotted line), increases exponentially with r_0 . Parameters: $D = v = 1$ and $\rho_0 = 4$.

nite domains drift randomly.

Motility-induced pinning – Numerical data shown in Figs. 1 and 2 suggest that the AIM exhibits only a crossover, not a sharp liquid-gas transition. The global polar order is hindered by the droplet excitation [48]. We will demonstrate, however, that these traveling droplets cease to exist as the inverse temperature β increases further, and the system undergoes a MIP transition. As β increases, two distinct time scales emerge: one for spin flips (fast process with rate $\sim e^\beta$) and the other for particle motion (slow process with rate $4D+v$). This separation of time scales significantly impacts droplet dynamics.

Consider the limiting case $\beta \rightarrow \infty$, where all particles on a site are in the same spin state. When a particle moves to a nonempty site, the particle's spin instantly aligns with the polarization at the target site. Consider two local domains of opposite polarization, one with positive magnetization on the left and another with negative magnetization on the right, confronting each other with a domain wall or an interface separating them. Particles near the interface exhibit a back-and-forth oscillation: whenever a particle self-propels across the interface, it flips its self-propulsion direction and returns, and this process repeats. Consequently, the interface will be pinned in space. In analogy to the resonance structures found in chemical bonds [51], this oscillating motion will be called resonance. When $v = 0$ (without self-propulsion), the resonance disappears, and the interfaces are never pinned. In 1D, a pinned interface becomes a point defect, which is called an aster [52].

The MIP phenomenon persists for finite values of β , as demonstrated in Fig. 3 (a). At $\beta = 5$, the system, starting from a random initial state, reaches a steady state with pinned interface segments. Figure 3 (a) also reveals a flux

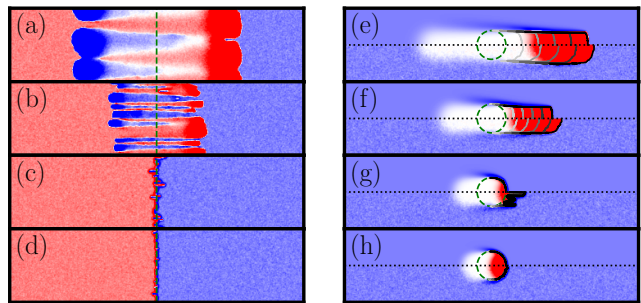


FIG. 4. Snapshots taken at 5×10^3 MCS after starting from a spanning domain wall (a-d) and a droplet of radius $r_0 = 50$ (e-h). The particle density within the droplet is 5 times higher than the background density. Panels cover a local area of size 1024×256 of the entire 4096×1024 lattice. In (e-h), both Monte Carlo simulation results (bottom half) and the numerical solutions of the hydrodynamic equation (top half), separated by dotted lines, are shown. The positions of the droplet front at $n \times 10^3$ MCSs ($n = 1, 2, 3, 4$) are also indicated [50]. Simulation parameters are $D = v = 1$, $\rho_0 = 4$, and varying $\beta = 3.0, 3.5, 4.0$, and 4.5 (top to bottom rows). Dashed lines represent the initial domain boundaries.

of particles among pinned interface segments. Individual particles exhibit both diffusive motion, at rate D , along pinned interfaces and the resonant motion. Upon reaching an edge, they leak out and flow until being captured by another segment. The steady state thus consists of a network of pinned interface segments where particle loss and gain due to the leak current are balanced. This is a unique feature of the system in dimensions higher than 1.

At $\beta = 5$, the line density l_p of the pinned segments in the steady state converges to a finite value as the system size increases (see Fig. 3 (b)). In contrast, it decreases at $\beta = 3$, where the system is supposed to be in an unpinned phase. The MIP transition is expected to occur at a threshold value near $\beta = 4$.

Interface dynamics also provides an evidence for the MIP transition. We study the time evolution of a spanning interface at $x = L_x/2$. It initially separates domains of positive magnetization on the left and negative magnetization on the right. When β is small, droplets nucleate at the interface and penetrate into the opposite domains (see Figs. 4(a, b)). Consequently, the interface width grows linearly with time. On the other hand, for large values of β , the MIP occurs and the interface width saturates to a finite value (see Figs. 4(c,d)).

An interface enclosing an isolated circular droplet exhibits similar behaviors (see Fig. 4(e-h)). To pinpoint the MIP transition point, we measure the traveling speed c_f of the front interface of the droplet. The speed, shown in Fig. 5(a), exhibits a discontinuous jump to zero at the critical value $\beta = \beta_c$. The phase diagram in the $D - 1/\beta$ plane, based on the threshold values β_c obtained from

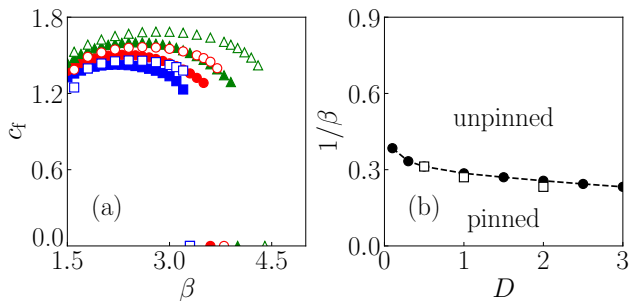


FIG. 5. (a) Speed of the front interface of a droplet. Results from the Monte Carlo simulations on a 4096×512 lattice (empty symbols) are compared with those from the hydrodynamic equation (filled symbols). Data are shown for $D = 0.5$ (square), 1.0 (circle), and 2.0 (triangle). (b) Phase diagram. Transition points are determined from the Monte Carlo simulations (empty symbols) and the hydrodynamic equation (filled symbols). The Dashed line is a guide for the eye. In all cases, $v = 1$ and $\rho_0 = 4$.

different diffusion rates D , is presented in Fig. 5(b).

In the pinned phase, an isolated droplet of radius r_0 eventually evaporates due to the leak current in a characteristic life time $\tau(r_0)$. The life time seems to grow exponentially with r_0 (see Fig. 3(c)). We speculate that this exponential growth, along with the network of leak currents, may be crucial for the MIP phase, which requires further investigations.

MIP from hydrodynamic theory – The MIP transition is also captured by the hydrodynamic equation (1). The space-discretized version exhibits both traveling and pinned droplet solutions (see Fig. 4). The interface speed from the hydrodynamic equation also shows a discontinuous jump at β_c . The speed and the resulting phase diagram are in a qualitative agreement with those obtained from the microscopic model (see Fig. 5).

We note that the hydrodynamic theory of Ref. [48] predicts a traveling droplet solution only. We revisit the hydrodynamic theory to reconcile it with the phenomenon of MIP. Consider a droplet of density ρ_d and magnetization $m_d = p\rho_d > 0$, whose front moves at a constant speed c_f on an ordered background characterized by particle density ρ_o and magnetization $m_o = -p\rho_o < 0$. The polarization $p > 0$ is determined by $p = \tanh \beta p$. Mass conservation requires that $c_f = \frac{m_d + |m_o|}{m_d - |m_o|} pv = \frac{\rho_d + \rho_o}{\rho_d - \rho_o} pv$. Using a Newton mapping [53, 54] combined with a small density gradient expansion $\rho \simeq \rho_o + v[m - m_o]/c_f$ [48], the hydrodynamic equation leads to a simplified description for the magnetization $m(z)$ along the symmetry axis of a droplet:

$$D_x \frac{d^2 m}{dz^2} = -\gamma(c_f) \frac{dm}{dz} - \frac{dV(m; c_f)}{dm}, \quad (2)$$

where $z = x - c_f t$ is the coordinate in the comoving frame, $\gamma(c_f) = c_f - v^2/c_f$, and $V(m; c_f) = \int F(\rho_o + v(m -$

$m_o)/c_f, m) dm$ [see Ref. [48] for detailed derivation]. Regarding m as a coordinate and z a time, this equation describes a damped motion of a particle of mass D_x under the inverted double-well potential $V(m; c_f)$. This potential has two unstable fixed points at $m = m_o$ and m_d with a potential difference $\Delta V \equiv V(m_d; c_f) - V(m_o; c_f)$. The traveling droplet solution corresponds to the heteroclinic orbit connecting these two unstable fixed points. The condition that the excess potential energy ΔV is exactly dissipated by the damping term determines the propagation speed c_f self-consistently.

When β and c_f are large, the self-consistent equation admits an approximate solution. Due to mass conservation, we have $\Delta \rho := \rho_d - \rho_o = 2vp\rho_o/c_f + O(c_f^{-2})$ and $\Delta|m| := m_d - |m_o| = 2vp^2\rho_o/c_f + O(c_f^{-2})$. We can set the polarization $p = 1$ neglecting an $O(e^{-2\beta})$ correction. Keeping only the leading order term in the integral $\Delta V = \int_{m_o}^{m_d} F dm$, we obtain

$$\Delta V = \frac{6v\rho_o^2}{\beta^2 c_f} e^\beta (1 + O(\beta^{-1}, c_f^{-1})). \quad (3)$$

The energy dissipation $E_d = \frac{1}{2} \int_{-\infty}^{\infty} \gamma|m'(z)|^2 dz$ is approximated as $E_d \simeq \gamma(m_d - m_o)^2/\Delta z$, where Δz denotes a time required for a transition from m_d to m_o . When $|\delta m| \ll 1$ with $\delta m := m - m_o$, Eq. (2) becomes

$$D_x \delta m'' \simeq -\gamma \delta m' + k \delta m \quad (4)$$

with a stiffness constant $k = -\frac{dF}{dm}|_{m=m_o} \simeq e^\beta$. Assuming $\delta m \sim e^{-z/\tau_z}$ with $\tau_z > 0$, we obtain

$$\tau_z = \frac{2D_x}{\gamma + \sqrt{\gamma^2 + 4D_x k}}. \quad (5)$$

Therefore, the transition time is given by $\Delta z = a\tau_z$ with $O(1)$ constant a . Equating the excess potential energy and the energy dissipation, we finally obtain that

$$c_f \simeq \left(3av\sqrt{D_x/2}\right)^{1/2} \beta^{-1} e^{\beta/4}. \quad (6)$$

The exponential dependence is consistent with the numerical solution of Eq. (2) (not shown here).

The growing density gradient, $\Delta\rho/\Delta z \sim e^{\beta/4}$, associated with the traveling droplet solution, makes the density gradient expansion worse and worse as β increases. We will argue that the traveling droplet solution breaks down beyond a threshold β_c using the resonance mechanism. We consider a simplified model consisting of only two sites A and B , representing locations on the left and right of the droplet's front interface, respectively. During a time interval $\tau_f = e^{-\beta}$, $f_+ = \rho_d(D + v)\tau_f$ particles of positive spin flow from A to B , while $f_- = \rho_o(D + v)\tau_f$ particles of negative spin flow from B to A . We choose a specific value $\tau_f = e^{-\beta}$ so that spin flips are suppressed during this time interval. The droplet can move forward only if the invading particles (f_+) outnumber the remaining

particles ($\rho_o - f_-$) at B . Otherwise, the invaders reverse their spin states and return back to site A , starting the resonating motion. Therefore, the traveling droplet solution requires $f_+ > \rho_o - f_-$, which imposes an upper bound for c_f :

$$c_f < v / (1 - 2(D + v)e^{-\beta}). \quad (7)$$

For large β , this bound decreases whereas the solution in Eq. (6) increases with β . This inconsistency implies the existence of a threshold value β_c , beyond which the resonance sets in and interfaces become pinned.

Discussions – We have discovered a novel phenomenon of MIP in the AIM. Pinning typically occurs due to defects or impurities in various systems, including magnetic systems, fluctuating surfaces, and active matters [33, 36, 55–57]. Our work reveals a unique mechanism for pinning in the absence of any quenched disorder: a resonating back-and-forth motion of SPPs.

Contrary to early expectations [24, 45, 46], the AIM does not exhibit a long-range polar order. For $\beta < \beta_c$, the order is short-ranged in both space and time due to drifting finite domains. For $\beta > \beta_c$, pinned interfaces emerge, and trap particles and emit a particle current at random directions at their edges. This leaking current generates a short-range polar order in space. However, a specific configuration of the leaking current persists up to the life time of pinned interfaces. Therefore, the MIP provides a mechanism for a long-range polar order in time.

We have also studied the active p -state clock model, in which the self-propulsion direction is modeled with p -state clock spins. We observed the MIP for $p \leq 4$ [50]. These results will be presented elsewhere.

-
- [1] M. C. Marchetti, J.-F. Joanny, S. Ramaswamy, T. B. Liverpool, J. Prost, M. Rao, and R. A. Simha, Hydrodynamics of soft active matter, *Reviews of Modern Physics* **85**, 1143 (2013).
- [2] C. Bechinger, R. Di Leonardo, H. Löwen, C. Reichhardt, G. Volpe, and G. Volpe, Active particles in complex and crowded environments, *Reviews of Modern Physics* **88**, 045006 (2016).
- [3] R. Di Leonardo, L. Angelani, D. Dell’Arciprete, G. Ruocco, V. Iebba, S. Schippa, M. P. Conte, F. Mecarini, F. De Angelis, and E. Di Fabrizio, Bacterial ratchet motors, *Proceedings of the National Academy of Sciences* **107**, 9541 (2010).
- [4] L. Huber, R. Suzuki, T. Krüger, E. Frey, and A. Bausch, Emergence of coexisting ordered states in active matter systems, *Science* **361**, 255 (2018).
- [5] S. Henkes, K. Kostanjevec, J. M. Collinson, R. Sknepnek, and E. Bertin, Dense active matter model of motion patterns in confluent cell monolayers, *Nature Communications* **11**, 1405 (2020).
- [6] J. Buhl, D. J. Sumpter, I. D. Couzin, J. J. Hale, E. Despland, E. R. Miller, and S. J. Simpson, From disorder to order in marching locusts, *Science* **312**, 1402 (2006).
- [7] I. Giardina, Collective behavior in animal groups: theoretical models and empirical studies, *HFSP Journal* **2**, 205 (2008).
- [8] M. Ballerini, N. Cabibbo, R. Candelier, A. Cavagna, E. Cisbani, I. Giardina, V. Lecomte, A. Orlandi, G. Parisi, A. Procaccini, *et al.*, Interaction ruling animal collective behavior depends on topological rather than metric distance: Evidence from a field study, *Proceedings of the national academy of sciences* **105**, 1232 (2008).
- [9] A. J. Ward, D. J. Sumpter, I. D. Couzin, P. J. Hart, and J. Krause, Quorum decision-making facilitates information transfer in fish shoals, *Proceedings of the National Academy of Sciences* **105**, 6948 (2008).
- [10] A. Cavagna and I. Giardina, Bird flocks as condensed matter, *Annu. Rev. Condens. Matter Phys.* **5**, 183 (2014).
- [11] A. Cavagna, D. Conti, C. Creato, L. Del Castello, I. Giardina, T. S. Grigera, S. Melillo, L. Parisi, and M. Viale, Dynamic scaling in natural swarms, *Nature Physics* **13**, 914 (2017).
- [12] A. Bricard, J.-B. Caussin, N. Desreumaux, O. Dauchot, and D. Bartolo, Emergence of macroscopic directed motion in populations of motile colloids, *Nature* **503**, 95 (2013).
- [13] N. Kumar, H. Soni, S. Ramaswamy, and A. Sood, Flocking at a distance in active granular matter, *Nature communications* **5**, 4688 (2014).
- [14] J. Yan, M. Han, J. Zhang, C. Xu, E. Luijten, and S. Granick, Reconfiguring active particles by electrostatic imbalance, *Nature Materials* **15**, 1095 (2016).
- [15] B. Liebchen and H. Lowen, Synthetic chemotaxis and collective behavior in active matter, *Accounts of Chemical Research* **51**, 2982 (2018).
- [16] T. Vicsek, A. Czirók, E. Ben-Jacob, I. Cohen, and O. Shochet, Novel type of phase transition in a system of self-driven particles, *Physical Review Letters* **75**, 1226 (1995).
- [17] J. Toner and Y. Tu, Long-range order in a two-dimensional dynamical xy model: how birds fly together, *Physical Review Letters* **75**, 4326 (1995).
- [18] N. D. Mermin and H. Wagner, Absence of ferromagnetism or antiferromagnetism in one- or two-dimensional isotropic heisenberg models, *Physical Review Letters* **17**, 1133 (1966).
- [19] Y. Fily and M. C. Marchetti, Athermal phase separation of self-propelled particles with no alignment, *Physical Review Letters* **108**, 235702 (2012).
- [20] I. Buttinoni, J. Bialké, F. Kümmel, H. Löwen, C. Bechinger, and T. Speck, Dynamical clustering and phase separation in suspensions of self-propelled colloidal particles, *Physical Review Letters* **110**, 238301 (2013).
- [21] M. E. Cates and J. Tailleur, Motility-induced phase separation, *Annu. Rev. Condens. Matter Phys.* **6**, 219 (2015).
- [22] L. Caprini, U. M. B. Marconi, and A. Puglisi, Spontaneous Velocity Alignment in Motility-Induced Phase Separation, *Physical Review Letters* **124**, 078001 (2020).
- [23] Z. Csahók and T. Vicsek, Lattice-gas model for collective biological motion, *Physical Review E* **52**, 5297 (1995).
- [24] A. P. Solon and J. Tailleur, Revisiting the flocking transition using active spins, *Physical Review Letters* **111**, 078101 (2013).
- [25] M. Mangeat, S. Chatterjee, R. Paul, and H. Rieger, Flocking with a q-fold discrete symmetry: Band-to-lane transition in the active potts model, *Physical Review E* **102**, 042601 (2020).

- [26] S. Chatterjee, M. Mangeat, R. Paul, and H. Rieger, Flocking and reorientation transition in the 4-state active potts model, *Europhysics Letters* **130**, 66001 (2020).
- [27] F. Dittrich, T. Speck, and P. Virnau, Critical behavior in active lattice models of motility-induced phase separation, *The European Physical Journal E* **44**, 1 (2021).
- [28] A. Solon, H. Chaté, J. Toner, and J. Tailleur, Susceptibility of polar flocks to spatial anisotropy, *Physical Review Letters* **128**, 208004 (2022).
- [29] S. Chatterjee, M. Mangeat, and H. Rieger, Polar flocks with discretized directions: the active clock model approaching the vicsek model, *Europhysics Letters* **138**, 41001 (2022).
- [30] A. M. Menzel, Collective motion of binary self-propelled particle mixtures, *Physical Review E* **85**, 021912 (2012).
- [31] M. Fruchart, R. Hanai, P. B. Littlewood, and V. Vitelli, Non-reciprocal phase transitions, *Nature* **592**, 363 (2021).
- [32] S. Chatterjee, M. Mangeat, C.-U. Woo, H. Rieger, and J. D. Noh, Flocking of two unfriendly species: The two-species vicsek model, *Physical Review E* **107**, 024607 (2023).
- [33] O. Chepizhko and F. Peruani, Diffusion, Subdiffusion, and Trapping of Active Particles in Heterogeneous Media, *Physical Review Letters* **111**, 160604 (2013).
- [34] S. Ro, Y. Kafri, M. Kardar, and J. Tailleur, Disorder-Induced Long-Ranged Correlations in Scalar Active Matter, *Physical Review Letters* **126**, 048003 (2021).
- [35] Y. Duan, B. Mahault, Y.-q. Ma, X.-q. Shi, and H. Chaté, Breakdown of ergodicity and self-averaging in polar flocks with quenched disorder, *Physical Review Letters* **126**, 178001 (2021).
- [36] D. Vahabli and T. Vicsek, Emergence of synchronised rotations in dense active matter with disorder, *Communications Physics* **6**, 56 (2023).
- [37] J. Toner and Y. Tu, Flocks, herds, and schools: A quantitative theory of flocking, *Physical Review E* **58**, 4828 (1998).
- [38] G. Grégoire and H. Chaté, Onset of collective and cohesive motion, *Physical Review Letters* **92**, 025702 (2004).
- [39] E. Bertin, M. Droz, and G. Grégoire, Boltzmann and hydrodynamic description for self-propelled particles, *Physical Review E* **74**, 022101 (2006).
- [40] H. Chaté, F. Ginelli, G. Grégoire, and F. Raynaud, Collective motion of self-propelled particles interacting without cohesion, *Physical Review E* **77**, 046113 (2008).
- [41] H. Chaté, F. Ginelli, G. Grégoire, F. Peruani, and F. Raynaud, Modeling collective motion: variations on the vicsek model, *The European Physical Journal B* **64**, 451 (2008).
- [42] E. Bertin, M. Droz, and G. Grégoire, Hydrodynamic equations for self-propelled particles: microscopic derivation and stability analysis, *Journal of Physics A: Mathematical and Theoretical* **42**, 445001 (2009).
- [43] G. Baglietto and E. V. Albano, Nature of the order-disorder transition in the vicsek model for the collective motion of self-propelled particles, *Physical Review E* **80**, 050103 (2009).
- [44] T. Ihle, Invasion-wave-induced first-order phase transition in systems of active particles, *Physical Review E* **88**, 040303 (2013).
- [45] A. P. Solon and J. Tailleur, Flocking with discrete symmetry: The two-dimensional active ising model, *Physical Review E* **92**, 042119 (2015).
- [46] A. P. Solon, H. Chaté, and J. Tailleur, From phase to microphase separation in flocking models: The essential role of nonequilibrium fluctuations, *Physical Review Letters* **114**, 068101 (2015).
- [47] J. Codina, B. Mahault, H. Chaté, J. Dobnikar, I. Pagonabarraga, and X.-q. Shi, Small obstacle in a large polar flock, *Physical Review Letters* **128**, 218001 (2022).
- [48] B. Benvegnen, O. Granek, S. Ro, R. Yaacoby, H. Chaté, Y. Kafri, D. Mukamel, A. Solon, and J. Tailleur, Metastability of Discrete-Symmetry Flocks, *Physical Review Letters* **131**, 218301 (2023).
- [49] We confirmed that the results are qualitatively the same under the parallel update and the random sequential update.
- [50] See also a movie in Supplemental Material.
- [51] P. Muller, Glossary of terms used in physical organic chemistry (IUPAC Recommendations 1994), *Pure and Applied Chemistry* **66**, 1077 (1994).
- [52] B. Benvegnen, H. Chaté, P. L. Krapivsky, J. Tailleur, and A. Solon, Flocking in one dimension: Asters and reversals, *Physical Review E* **106**, 054608 (2022).
- [53] J.-B. Caussin, A. Solon, A. Peshkov, H. Chaté, T. Dauxois, J. Tailleur, V. Vitelli, and D. Bartolo, Emergent Spatial Structures in Flocking Models: A Dynamical System Insight, *Physical Review Letters* **112**, 148102 (2014).
- [54] A. P. Solon, J.-B. Caussin, D. Bartolo, H. Chaté, and J. Tailleur, Pattern formation in flocking models: A hydrodynamic description, *Physical Review E* **92**, 062111 (2015).
- [55] F. Peruani and I. S. Aranson, Cold Active Motion: How Time-Independent Disorder Affects the Motion of Self-Propelled Agents, *Physical Review Letters* **120**, 238101 (2018).
- [56] P. Forgács, A. Libál, C. Reichhardt, and C. J. O. Reichhardt, Active matter shepherding and clustering in inhomogeneous environments, *Physical Review E* **104**, 044613 (2021).
- [57] G. K. Sar, D. Ghosh, and K. O’Keeffe, Pinning in a system of swarmalators, *Physical Review E* **107**, 024215 (2023).

Supplemental Materials for “Motility-Induced Pinning in Flocking System with Discrete Symmetry”

Chul-Ung Woo and Jae Dong Noh

Department of Physics, University of Seoul, Seoul 02504, Korea

- File `1_nucleation_homogeneous.mp4` corresponds to the supplementary movie for Fig. 1. It shows a time evolution of the microscopic model from a homogeneous ordered state to a state with nucleated droplets. Parameters: $L_x = L_y = 4086, \rho_0 = 8, \beta = 2, v = 1, D = 0.05$.
- File `2_nucleation_band.mp4` corresponds to the supplementary movie for Fig. 2 showing a time evolution of the microscopic model from a macrophase separated state to a state with nucleated droplets. Parameters: $L_x = 2048, L_y = 256, \rho_0 = 3, \beta = 2, v = 1, D = 0.1$.
- File `3_MIP.mp4` corresponds to the supplementary movie for Fig. 3. demonstrates the time evolution into the motility-induced pinning phase in the microscopic model. Parameters: $L_x = L_y = 4096, v = 1, D = 1, \beta = 5, \rho_0 = 4$.
- Files `4_droplet.mp4` and `5_droplet_DHE.mp4` are the supplementary movies for Fig. 4. They show the time evolution of an isolated circular droplet in the ordered background in the microscopic model and the discretized hydrodynamic equation, respectively. Parameters: $L_x = 1024, L_y = 256, v = 1, D = 1, \rho_o = 4, r_0 = 50$.
- File `6_ACM_droplet.mp4` is the supplementary movie for the last paragraph of the main text. It shows the motion of pinned and unpinned droplets in the active p -state clock model with $p = 4$ (left column) and $p = 8$ (right column) in the microscopic model (top row) and in the discretized hydrodynamic equation (bottom row). Parameters: $L_x = L_y = 1024, \rho_o = 10, \beta = 6, v = 1, D = 1$.